Physicists in Industry (5)

A Useful SW Tool for Thermal Estimations in Optics

Beat Aebischer and Bernhard Braunecker

Introduction

Physicists in industry very often have to take fast decisions, if e.g., specifications run out of tolerance in production, and one has to look rapidly for compensation means in the production chain. Since in most cases, there is not sufficient time to analyze the problem seriously, the decisions taken are more or less intuitive with the risk of leading to suboptimal solutions. Another stressful situation, especially in the optics industry, occurs when starting work on a new system layout. If the system specifications include operations under harsh environmental conditions, the designer has to identify the glass materials for the lenses as soon as possible due to their long delivery times. Since only a preliminary design exists at this early phase of the development, the selection of the expensive glasses bares some risk.

We have therefore developed a special SW tool for physically relevant estimations to manage better both unpleasant situations. Its purpose is to bridge the gap between pure intuition/experience and a full numerical Finite Element calculation. The results are approximations, but they at least point into the right physical direction. We wrote the SW in Matlab to allow easy case adaptions and plausibility checks. Further advantages are that the program runs on a portable laptop, and that the results are immediately available. In the following, we describe the physical models, which we used for thermal estimations in three optical projects. In the publication [1] we present the mathematical concept and the solutions for the first two applications (photogrammetric lenses, satellite terminals), while we treat the third application about laser processing in the following here in more detail.

Application 1: Photogrammetric Lenses

Leica Geosystems, former Wild Heerbrugg, produces big objective lenses for airborne photogrammetric cameras since many decades. Most prominent in the past was the *Reihenkamera* RC30 (see Box III), equipped with the *Ultra Aviogon Super 15/4 UAGS* (Fig. 1). The lens has a focal length of 153 mm, F-number 4, a field of view of 90°, and is exposing 9-inch square film in the visual and infrared spectral range. The cameras recorded nearly every square-meter of our earth on high-resolution photographic
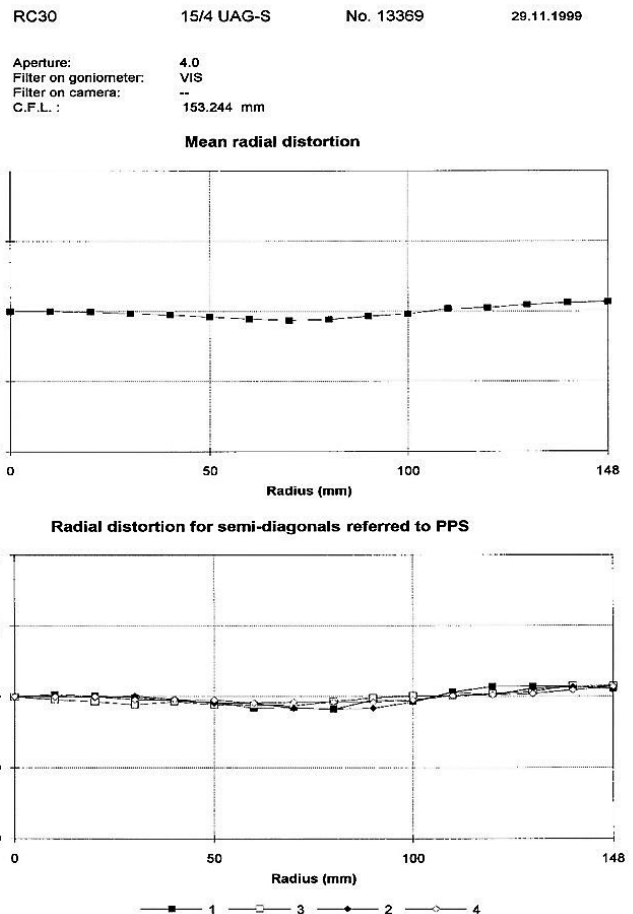

Fig. 2: Distortion error across the four semi-diagonals of a 9" square film.
a) Average b) the 4 individual semi-diagonals. No splitting allowed.

film. We see from Fig. 2 that the distortion error must be kept within ±2 μm in the film plane for all four semi-diagonals of 153 mm length, a requirement hard to achieve in production [2].

The technical construction drawing (Fig. 3) shows that the big lenses of up to 300 mm diameter are glued in the cylindrical housing with minimal mechanical contact to avoid any deformation of the strongly bended spherical surfaces. On the other hand, the mechanical mount must be stable enough to survive heavy shocks and vibrations from the airplane. To find the right balance needs a lot of experience in optical engineering.

Thermal Gradients in Large Scale Optics

The film lenses and their digital follow-up versions operate within the large temperature range from -30°C to +60°C. Therefore, one always had to consider athermalization

1 Heat Conduction in Lenses, Beat Aebischer; Hindawi Publishing Corporation; Mathematical Problems in Engineering, Vol 2007, Article ID 57360; doi:10.1155/2007/57360

2 We also note in Fig. 1 another technical challenge, the round pupil: The exit pupil must be non-obscured like a cat's eye, even under the large observation angle of 45°. The measurements confirm that the light fall-off at this field angle is 0.66, according to a $\cos^{1.2}$-law. This is a significant and non-trivial improvement, compared to the usual $\cos^4$-law, which would lead to only 0.25.

I: Passive Athermalization

To illustrate an example of a widely used passive method, we consider the simple case of two single lenses. The two radii of curvature, the glass thickness and the refractive indices of both lenses vary with temperature and cause an image defocus, which we can compensate by changing appropriately the air gap between the lenses. To this purpose, we fix the second lens on a special mount consisting of two materials with different thermal expansion coefficients, like Al and Invar, which is an old Swiss watchmaker's trick to keep the length of a pendulum independent of temperature.
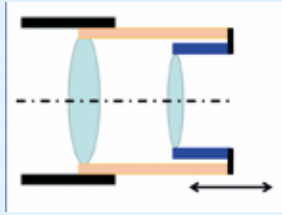
Shifting two lens groups allows to correct besides defocus also the magnification, i.e. the focal length. The shifting values are typically 1.5 $\mu m/°C$. It is interesting to note that the famous glass ceramics Zerodur© of Schott AG, often used in astronomical mirrors due to its zero thermal expansion, is a mixture of two material phases, a crystalline one with negative thermal expansion coefficient and an amorphous one with positive coefficient. Swiss watchmaker technique in 3 dimensions!
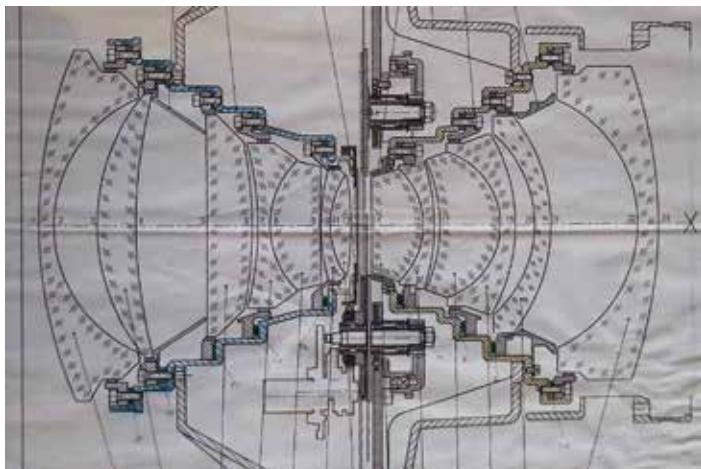

*Fig. 3: Constructive details of an earlier **UAGS** version. The film plane is directly behind the right lens (see Fig. 5).*

techniques to maintain the optical quality within the large temperature range. A standard method is described in Box I. However, the compensation only holds for *stationary* thermal conditions, i.e. when all parts are at the same new temperature. But what happens, when the user starts from an airport in the desert at a temperature of +60°C and reaches after few minutes a flying height of 5000 m, where the temperature drops down to about -30°C? This causes strong thermal gradients of the refraction index across the diameter of the big lenses, degrading the image sharpness and the carefully minimized distortion. Thus we were asked how strong and how long optical gradients in the glass material would deteriorate the image quality?

Modeling Heat Transfer

We model each optical element as a thin disk of radius R with rotational symmetry, ignoring its true 3D-shape. Then

we obtain analytic solutions of the heat flow and the resulting temperature profile across the disk area with time. On the other hand, we exactly describe constraints like e.g. how, when and how long external heat is switched on, and we always use the correct material data of the glass disk and the glue, with which the disk is fixed in a metallic housing [3]. The diffusion time $t_c = R^2/\kappa$ is of central importance, where $\kappa = \lambda/(c_p\,\rho)$ is the thermal diffusivity in [m²/s], using the heat conductivity λ in [W/m/K], the specific heat (at constant pressure) c_p in [J/kg/K], and the density of the material ρ in [kg/m³]. For Schott glass N-BK7 with $\lambda = 1.114$ W/m/K, $c_p = 858.0$ J/kg/K and $\rho = 2.5 \cdot 10^3$ kg/m³ one obtains $\kappa = 5.2 \cdot 10^{-7}$ m²/s, while other common glasses like N-FK5 and N-LAF7 yield $4.7 \cdot 10^{-7}$ m²/s and $3.6 \cdot 10^{-7}$ m²/s, respectively.

Examples

We consider the temperature distribution as function of time across a cold glass disk, initially kept at -30°C and brought to an environment of +40°C. The material is Schott glass
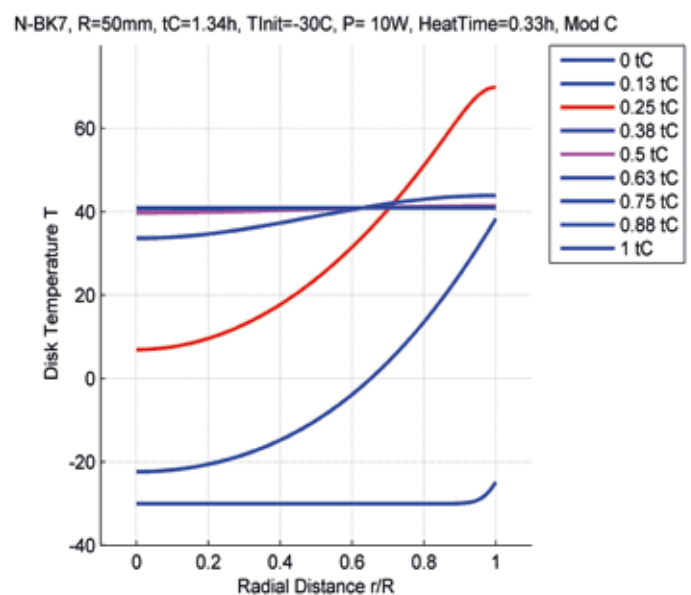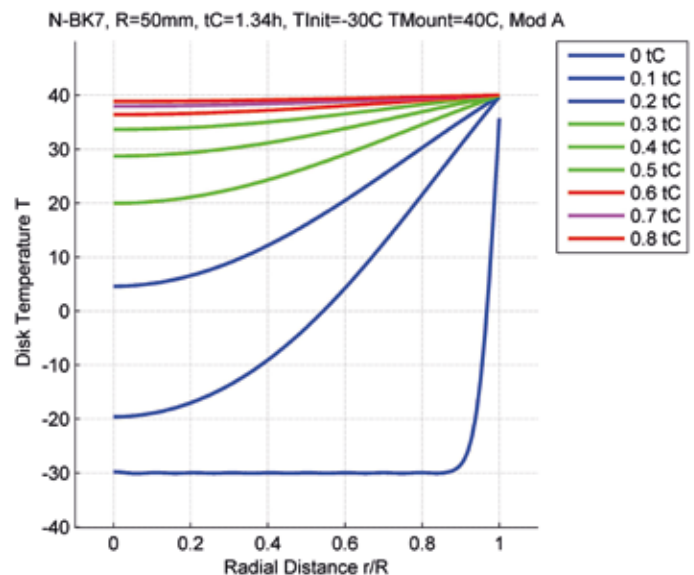

Fig. 4: Temperature distribution across a disk of radius R = 50 mm for different times t/t_c.
a) Pure diffusion, b) Heating 10 W for 20 minutes.

3 The differential equations, their analytical solutions, and several numerical examples are described in full detail in the publication cited in Footnote 1.

N-BK7, and when assuming a disk radius $R = 50$ mm, we obtain from above the surprisingly large value $t_c = R^2/\kappa = 1.34$ h [4]. The disk is glued into a metal ring, which carries a heating coil.

It can be seen in Fig. 4a that we need the time t_c to reach the thermal equilibrium by heat diffusion. In Fig. 4b we want to speed up the warming and apply $P = 10$ W of heating power for 20 minutes by the coil. Then the final state is reached after about $0.5 \cdot t_c$ (magenta line), but with a temperature peak at the disk rim of about +70°C at the end of the heating interval (red line). What does this mean optically?

Temporary Optical Aberrations

Let us consider the ray refraction at the surface of a spherical lens with radius of curvature r_{Surf}, glass thickness d and index of refraction n. All three quantities depend on temperature: r_{Surf} and d by the thermal expansion coefficient of the glass material, and n by the empirical *Sellmeier* formula. Before tracing a ray through the lens surface at the lateral position r and at time t, we calculate the glass temperature T and correct r_{Surf}, d, and n accordingly.

We compare two image points in Fig. 5: the first one on-axis, i.e. in the center of the image plane, and the other one off-axis, i.e. lying at the edge of the image plane. The light rays of the off-axis pixel cross most of the big lenses at the periphery, where the temperature quickly reaches the environmental value, while the rays of a central pixel stay close to the axis.
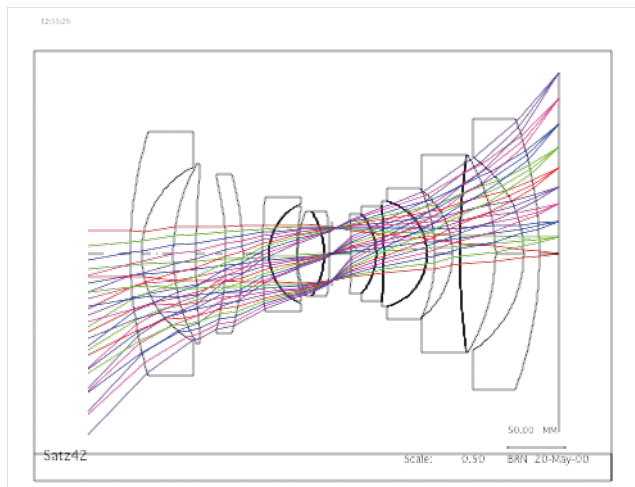

Fig. 5: UAGS-2, Design

When combined with the already mentioned mechanical movement along the optical axis of several lens groups, the off-axis image point thus will keep its best focus position. This is, however, different for the pixel in the central part, where the optical path crosses the inner lens segments, which reach the environmental temperature only later. This leads to a defocus varying with time. We therefore obtain some kind of *image curvature* for times shorter than typical values of t_c. Active heating and cooling would obviously shorten the time for the inner pixels to reach the thermal equilibrium, but at the cost of counterproductive over-heating at the rim zones (Fig. 4b). Thus our simple thermal modeling indicates that we had to flush the large lenses of the film camera by ambient air. This is different in the case of the

digital cameras, where the lenses are of smaller diameter. They are mounted in a sealed housing, filled with protection gas, and the mechanical lens shifting (Box I) is part of the construction. We also introduced in the lens design a special aberration to efficiently manage thermal gradients at white light illumination [5].

All these considerations have to be made before the design work starts which can last several months. Nevertheless, the most reliable, but also expensive solution is to *overdesign* the lens performance (resolution, contrast, distortion) to master the quality degradation, at least for smaller temperature differences.

Application 2: Satellite Terminals

Here is another problem, now in connection with space telescopes, which send and receive laser radiation. The telescopes could be e.g. part of a laser altimeter for the exploration of a planet (Fig. 6), or of a laser communication system between two orbiting satellites [6]. The problem is to guide the laser beam with minimal loss through the optics, but to reject the incident solar radiation. Unwanted solar background radiation can result from reflections from earth's or the planet's surface, or from the sun suddenly appearing within the field of view of one of the communication terminals.
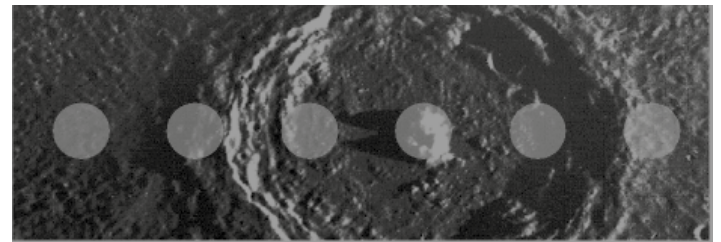

Fig. 6: Simulated Laserspots of 100 m diameter on Mercury, emitted from a 1000 km orbit with 10 Hz repetition frequency. The ground speed of the laser spot is 1.816 km/s.

Since the narrow band surface coating of all components within the optical path unavoidably has some residual absorption, one has to know the amount of the absorbed heat as function of time. The problem is similar to Application 1, since a time-variable thermal load can lead to gradients of the temperature across the component, causing defocusing of the laser radiation. Then the received and the emitted laser intensity can vary with time, which one has to know in case of an altimeter, or even to correct, when transmitting data, to keep the intensity dependent bit error rate constant.

In our SW tool we consider again a round filter glass of radius R and height h, which is glued in a cylinder mantle, kept at a constant temperature T_{Cyl}. We describe the sun illumination by a constant and homogeneous heat flux density q [W/m²], exposing the whole disk area for the time duration t_{Exp}. As an example we show in Fig. 7 the case of a glass

---

[4] A lens of 300 mm diameter would need $t_c = 12$ h.

[5] Most lenses for digital sensors are telecentric, i.e. the ray bundles hit the sensor at normal incidence. This allows designing the lenses with a small amount of longitudinal color aberration. Then thermally induced defocusing results only in a small spectral color shift for each pixel, but keeps the spot size and spot position.

[6] *http://www.sps.ch/artikel/physiker-in-der-industrie/optical-space-communication-information-transfer-from-point-to-point-reinhard-h-czichy-synopta-gmbh-st-gallen-2/*
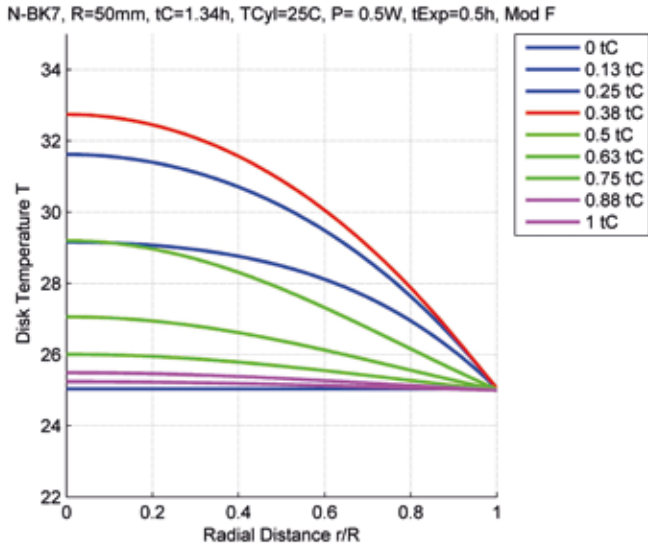
Fig. 7: Homogeneous exposure of a N-BK7 disk of radius R = 50 mm by 0.5 W for 30 minutes.

disk of N-BK7 of radius $R = 50$ mm, absorbing 0.5 W during 30 minutes. We see a general temperature increase until the heat switch-off time $t_{Exp} = 0.38 \cdot 1.34$ h = 0.5 h, where especially the disk center $r = 0$ raises up to 33°C. After ending the heat exposure, all parts reach the environmental temperature $T_{Cyl} = 25°C$ of the cylinder mantle. Now it is easy to estimate as function of time the change of the refractive index, the optical power of each optical element, and finally the defocusing.

Application 3: A Heat Conduction Problem in Connection with Laser Ablation

We consider a high power laser capable of producing very short (sub-μs) pulses concentrated in a small spot. The workpiece being hit by such a laser pulse is heated up almost instantaneously and the material is evaporated. To determine how much material is evaporated one must know where the temperature grows above a threshold, namely the evaporation or the sublimation temperature. This will allow us to determine the radius of a hole which the laser beam burns in different materials.

a) Temperature profile
For a single laser pulse hitting well inside a slab of homogeneous material, the process is so fast that the material boundary has almost no effect on the temperature. Also, if one wants to burn a hole with a single pulse, the material must be thin enough. We therefore model the workpiece as an infinite plate and homogenize the temperature with respect to the z-coordinate (orthogonal to the plate). The problem is then described by the two-dimensional heat equation $\partial u/\partial t = \kappa \Delta u$ with initial condition given by the heating up due to the pulse and κ [m²/s] the thermal diffusivity. It is reasonable to model the pulse as a **Gauss pulse** with total energy E_p and **full-width-half-maximum** (FWHM) b. Using polar coordinates centered in the laser spot, the energy hitting the material is distributed as

$$(1) \qquad e(r) = \frac{4 \ln 2 E_p}{\pi b^2} e^{-4 \ln 2 r^2 / b^2} \quad,$$

so that

$$2\pi \int_0^\infty e(r) \, r dr = E_p$$

is the total pulse energy. Assuming all the energy is absorbed, the **initial temperature** is

$$(2) \qquad u(r,0) = u_0 + \frac{e(r)}{c_p \rho h} \quad,$$

where c_p [J/kg/K] and ρ [kg/m³] are the specific heat and the density of the material, u_0 is the homogeneous temperature before the pulse hits, and h is the thickness of the plate. The temperature $u(r,t)$ is directly related to the two-dimensional euclidean **heat kernel**

$$(3) \qquad K(x,y;t) = \frac{1}{4\pi\kappa t} e^{-\|x-y\|^2/(4\kappa t)} \quad,$$

the fundamental solution of the heat equation for the initial condition (in the sense of distributions)

$$(4) \qquad \lim_{t \to 0} K(x,y;t) = \delta(x-y) = \delta_y(x) \quad.$$

From (1), (2), and (3), one sees that

$$(5) \qquad u(r,0) - u_0 = \frac{E_p}{c_p \rho h} K(x,0;t_b), \quad t_b = \frac{b^2}{16 \ln 2 \, \kappa}$$

and hence,

$$(6) \qquad \begin{aligned} u(r,t) - u_0 &= \frac{E_p}{c_p \rho h} K(x,0;t+t_b) \\ &= \frac{E_p}{c_p \rho h} \frac{1}{4\pi\kappa(t+t_b)} e^{-r^2/(4\kappa(t+t_b))} \quad. \end{aligned}$$

To express the solution in dimensionless form, we introduce **dimensionless variables** $\tilde{r}, \tilde{t}, \tilde{u}$:

$$(7) \qquad \begin{aligned} \tilde{r} &= \frac{r}{b}, \quad \tilde{t} = \frac{t}{T}, \quad \tilde{u}(\tilde{r},\tilde{t}) = \frac{u(r,t)-u_0}{U}, \\ T &:= \frac{b^2}{\kappa}, \quad U := \frac{E_p}{c_p \rho b^2 h} \quad, \end{aligned}$$
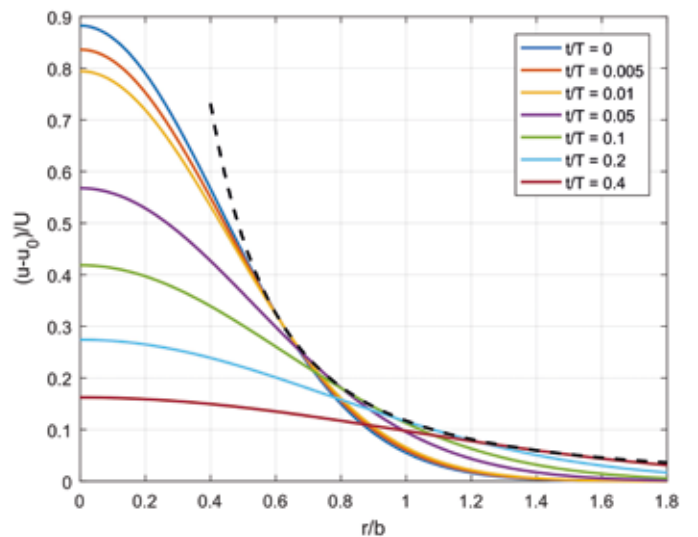
and get

Fig. 8: Solution (8) for different $\tilde{t}$, together with the envelope $1/(e\pi\tilde{r}^2)$, shown as the black dashed line.

$(8)\tilde{u}(\tilde{r},\tilde{t}) = \dfrac{1}{4\pi(\tilde{t}+\tilde{t}_b)}\,e^{-\tilde{r}^2/(4(\tilde{t}+\tilde{t}_b))}\,, \quad \tilde{t}_b = \dfrac{1}{16\ln 2} \approx 0.090168\,.$

(Choosing $U' = \kappa^2\rho h$ as the temperature scale would make the solution $\tilde{u}$ more complicated.)

Fig. 8 shows some numerical examples. For instance, $\tilde{u}(0,0) = 1/(4\pi\tilde{t}_b) = 4\ln 2/\pi \approx 0.88254\,.$

b) Maximal temperature after pulse arrival

At each radial coordinate the temperature reaches its maximum at a time $\tilde{t}$ determined by $\partial\tilde{u}/\partial\tilde{t} = 0$. This leads to the **envelope** shown in Fig. 8. Note, however, that for $\tilde{r} < 2\sqrt{\tilde{t}_b} = 1/\sqrt{4\ln 2} = 0{,}60056$ the envelope $1/(e\pi\tilde{r}^2)$ is due to curves $\tilde{u}(\tilde{r},\tilde{t})$ for negative $\tilde{t}$, which are not physically present. The maximal temperature reached at a given radial coordinate $\tilde{r}$ is therefore given by

$(9) \qquad \tilde{u}_{max}(\tilde{r}) = \max_{\tilde{t}\geq 0}\tilde{u}(\tilde{r},\tilde{t}) = \begin{cases} \tilde{u}(\tilde{r},0)\,, & \tilde{r}\leq 1/\sqrt{4\ln 2} \\ 1/(e\pi\tilde{r}^2)\,, & \tilde{r}\geq 1/\sqrt{4\ln 2} \end{cases}$

which is a monotonously decreasing function.

c) Radius of the burnt hole

We now consider a **threshold temperature** u_{thr}, e.g. the evaporation or sublimation temperature of the material and want to know for which radial coordinates r the maximal temperature u_{max} is above u_{thr}. As an estimate of the **radius of the hole** burnt by the laser pulse, one could use the value $\tilde{r}$ where $\tilde{u}_{max}$ reaches $\tilde{u}_{thr}$. However, this would largely overestimate the radius, because the heat of evaporation, which we did not take into account yet, greatly decreases the available energy!

We denote by $Q = Q_{melt} + Q_{ev}$ [J/K] the specific heat needed to melt and evaporate the material. The evaporation of a hole of radius $\tilde{r}$ then needs (in addition to heating up to u_{ev}) the energy

$(10) \qquad\qquad E_Q = \pi r^2 h\rho Q\,.$

II: Note on Nondimensionalization

The problem of the hole radius just discussed involves **11** physical parameters: E_p, b, h, ρ, Q_{melt}, Q_{ev}, u_{thr}, u_0, c_p, λ, κ. However, there are only **two** relevant nondimensional internal parameters that describe the whole process, e.g.

$(13) \qquad \tilde{u}_{thr} = \dfrac{u_{thr}-u_0}{E}c_p\rho b^2 h \text{ and } \tilde{Q} = \dfrac{Q_{melt}+Q_{ev}}{c_p(u_{thr}-u_0)}\,,$

since with the function $f_{11}:[0,\infty)\to[0,\infty)$ defined by equation (11) one can write

$(14) \qquad\qquad \tilde{r}\left(E_p = E\cdot(1 + \pi\tilde{r}^2\tilde{u}_{thr}\tilde{Q})\right) = f_{11}(\tilde{u}_{thr})\,.$

The parameter $\tilde{Q}$ is the quotient of the *latent* heat required to melt and evaporate the material in the hole and the *sensible* heat needed to bring the same material to the boiling point. For the metals appearing in Fig. 10 it ranges from 5 to 12. (Also $\tilde{u}_{thr}$ is a quotient of energies: the sensible heat needed to bring a volume b^2h to the boiling point and the excess energy $E = E_p - E_Q$.)

In reality, this energy is dissipated gradually as the hole forms and grows. A complete description of this process and its interaction with heat diffusion would involve a **free boundary problem**, which we cannot solve analytically. As a simple **approximation**, we let all of E_Q dissipate at the pulse arrival time $t = 0$ and allow only the **excess energy** $E = E_p - E_Q$ to diffuse as described by (8). This may underestimate the heat loss due to diffusion to the neighbouring material and therefore slightly overestimate the hole radius. Another effect in the same direction is that some pulse energy may not be absorbed. We still hope to get a reasonable approximation in most cases.

To **summarize** our approximation: Given E, compute $\tilde{r}$ from the condition $\tilde{u}_{max}(\tilde{r}) = \tilde{u}_{thr}$ with E_p replaced by E in (7) and with $u_{thr} = u_{ev}$. Then $r = \tilde{r}b$ is the hole radius corresponding to the pulse energy $E_p = E + E_Q$ (where E_Q depends on the radius r just determined).

The condition $\tilde{u}_{max}(\tilde{r}) = \tilde{u}_{thr}$ can only be satisfied if $\tilde{u}(0,0) \equiv 4\ln 2/\pi \geq \tilde{u}_{thr}$. Solving for $\tilde{r}$ (and using (8)) we thus get

$(11)\tilde{r} = \begin{cases} 0, & \tilde{u}_{thr}\geq c/\pi \\ \sqrt{\ln(c/(\pi\tilde{u}_{thr}))/c}, & c/(e\pi < \tilde{u}_{thr} < c/\pi \\ 1/\sqrt{e\pi\tilde{u}_{thr}}, & \tilde{u}_{thr}\leq c/(e\pi) \end{cases} \quad \begin{array}{l} c:= 4\ln 2 \\ e \equiv \exp(1) \end{array}$

The condition for a hole to form, $4\ln 2/\pi > \tilde{u}_{thr} \equiv (u_{thr}-u_0)/U$, is equivalent to

$(12) \qquad\qquad E_p > \dfrac{\pi}{4\ln 2}(u_{thr}-u_0)c_p\rho b^2 h =: E_{p,min}\,.$

For **iron** we use the approximate values
$\rho = 7870$ kg/m³, $c_p = 450$ J/kg/K, $\kappa = 2.3\cdot10^{-5}$ m²/s, $u_{ev} = 2862$°C, $Q_{melt} = 2.6\cdot10^5$ J/kg, $Q_{ev} = 6.1\cdot10^6$ J/kg.

With $b = 10$ μm, $h = 1$ mm, and $u_0 = 25$°C, we get $E_{p,min} = 1.14$ mJ.

Fig. 9 shows example plots of the approximate hole radius r as a function of the pulse energy E_p. As expected, the curves start to get positive at a threshold $E_{p,min}$, which for the
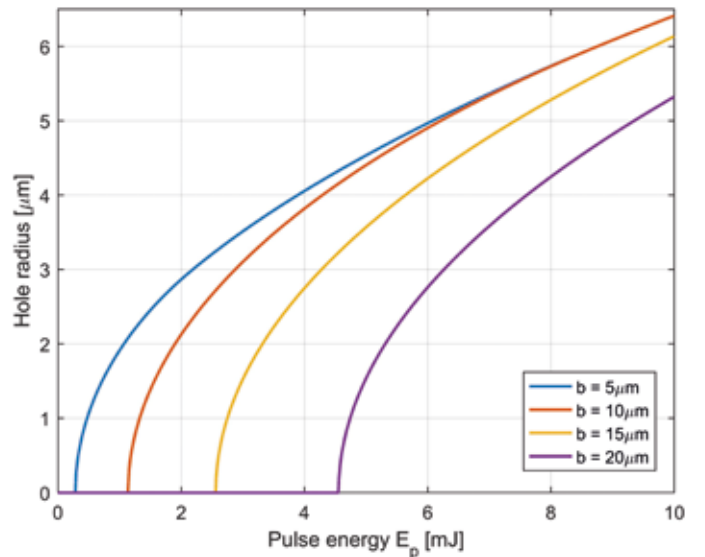

*Fig. 9: Hole radius r as a function of the pulse energy E_p for an **iron** sheet of thickness h = 1 mm. The pulse width (FWHM) b is given in the legend.*

red curve is the value 1.14 mJ given above. The plot clearly shows the advantage of focusing the pulse. Let us finally admit that assuming ρ, c_p, and κ to be constant from room to evaporation temperature is another simplification we have made. Please see the comment on the Nondimensionalization of the involved physical parameters in Box II.

d) Different materials

Based on the simulation we finally compare the exposure of different metal sheets of 1 mm thickness by a laser beam with Gaussian radius (FWHM) **b = 15 µm** and an applied pulse energy **E_p < 10 mJ**. The material data are taken from the web [7].

We see in Fig. 10 that the size of the burnt hole grows from the pair Fe/Cu to Ti and to the pair Al/Si. This ranking and the nearly identical behavior of Fe/Cu, respectively Si/Al, are surprising, since their physical data vary consid-
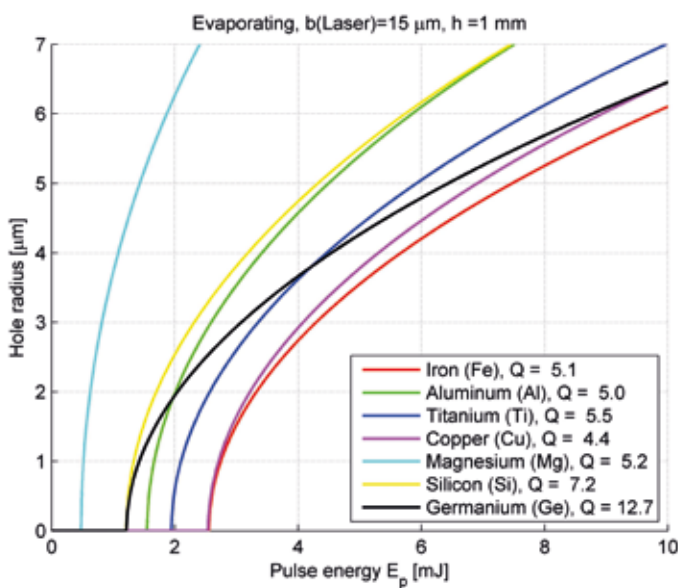

Fig. 10: The same as in Fig. 9, but for different materials, characterized by the nondimensional $\tilde{Q}$ of Box II.

---

7 http://periodictable.com/Properties/A/VaporizationHeat.st.log.html

erably. It indicates the complexity of the thermal process. The much larger hole radius when exposing Mg, however, is easier to explain, since its volume specific evaporation heat of 9.16 GJ/m^3 is 5.3 times smaller than that of iron with 48.9 GJ/m^3.

Final Remark

Describing real technical situations by simplified geometrical models allows analytical solutions of the involved physical mechanisms. We have shown concepts for three thermal diffusion processes. The advantage of closed solutions is a better understanding of the underlying physics, which is necessary to make the right decisions in the prephase of R&D work, or when problems occur in production. We are planning to extend our models to moving sheets of metal, ceramics and glass, exposed by time modulated ultra-short laser pulses. Results will/may be published in a later issue of this series.
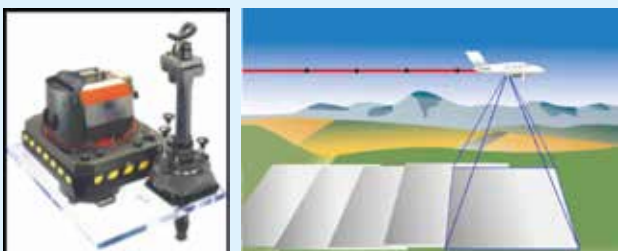
Beat Aebischer got a diploma in Theoretical Physics from the University of Bern and later a PhD in Mathematics from the same university. For 6½ years he has worked in pure mathematics, partly on a Swiss National grant at Yale University. In 1995 he joined the department *Product and Process Technology* of Leica Geosystems, Heerbrugg, which later became the *Hexagon Technology Center* (HTC).
His specialties are physical and mathematical modeling, signal processing, and calibration and compensation.

Hexagon AB offers a full palette of products in industrial metrology, terrestrial and aerial surveying, mining, and remote sensing. It was founded in 1992 in Stockholm and has incorporated Leica Geosystems in 2005. The Hexagon Technology Center (HTC) is its main laboratory for developing new technologies.

III: Analog Aerial Camera RC30

The film box of the *Reihenkamera* RC30 contained about 600 m high-resolution rollfilm. Pictures were recorded with (60 - 80)% overlap. The recording of the same ground pixel in adjacent film frames allowed to extract the height information by triangulation. The film transport was motorized and the film was pressed against the mechanical exposure frame, before the high-speed shutter opened. To compensate the forward motion blur the film frame was moved against the flight direction with the speed $v = v_{Ground} \cdot f / h$, where f is the focal length, h the flying height and v_{Ground} the speed over ground. The price of a RC30 was about 1 Mio CHF and about 400 units were sold worldwide.

Spatial resolution and Optical Transfer Function OTF of the lenses:
The resolution limit was set by the graininess of the used film material to 150 linepairs/mm in the visible and near IR spectrum, an important quantity for lower flying heights of about 500m. For larger flying heights of up to 3 km, where the atmosphere acts like a lowpass-filter for frequencies > 75 lp/mm, the OTF product of lens and atmosphere had to be maximized. This led to the demanding OTF value of 0.75 for the lenses.